




Fluorescence-activated cell sorting to reveal the cell origin of radioligand binding

Benjamin B Tournier¹ , Stergios Tsartsalis¹, Kelly Ceyzériat^{1,2},
Zadith Medina¹ , Ben H Fraser³, Marie-Claude Grégoire³,
Enikő Kövari^{4,5} and Philippe Millet^{1,5}

Abstract

Many studies have explored the role of TSPO (18 kDa translocator protein) as a marker of neuroinflammation using single-photon emission computed tomography (SPECT) or positron emission tomography (PET). In vivo imaging does not allow to determine the cells in which TSPO is altered. We propose a methodology based on fluorescence-activated cell sorting to sort different cell types of radioligand-treated tissues. We compared left/right hippocampus of rats in response to a unilateral injection of lipopolysaccharide (LPS), ciliary neurotrophic factor (CNTF) or saline. We finally applied this methodology in human samples (Alzheimer's disease patients and controls). Our data show that the pattern of TSPO overexpression differs across animal models of acute neuroinflammation. LPS induces a microglial expansion and an increase in microglial TSPO binding. CNTF is associated with an increase in TSPO binding in microglia and astrocytes in association with an increase in the number of microglial binding sites per cell. In humans, we show that the increase in CLINDE binding in Alzheimer's disease concerns microglia and astrocytes in the presence of a microglial expansion. Thus, the cellular basis of TSPO overexpression is condition dependent, and alterations in TSPO binding found in PET/SPECT imaging studies cannot be attributed to particular cell types indiscriminately.

Keywords

Alzheimer's disease, fluorescence-activated cell sorting, neuroinflammation, positron emission tomography/single-photon emission computed tomography, translocator protein

Received 5 January 2019; Revised 22 April 2019; Accepted 2 June 2019

Introduction

Molecular imaging has helped to better understand the pathophysiological processes of several oncological, neurodegenerative and psychiatric diseases. The in vivo measurement of the radioactive signal by single-photon emission computed tomography (SPECT) or positron emission tomography (PET) makes it possible to study the variations of the concentration of molecular targets with respect to various physiological and pathological processes. In Alzheimer's disease (AD) as in many psychiatric disorders, the presence of neuroinflammation, by the study of the 18 kDa translocator protein (TSPO), has been demonstrated.^{1–3} However, PET studies reported either AD-associated increases or no effect on TSPO density.^{4–11} In animal models, ex vivo quantification can be complementary to PET/SPECT imaging. It makes it possible to increase the sensitivity and the resolution of the measurement of

the radioactive signal. In humans and animals, in situ binding on slices or in vitro binding on homogenates (receptor binding assay) can also be performed from frozen samples.¹²

All these approaches enable quantification of the TSPO density at the tissue level, but provide no

¹Division of Adult Psychiatry, Department of Psychiatry, University Hospitals of Geneva, Geneva, Switzerland

²Division of Nuclear medicine, University Hospitals of Geneva, Geneva, Switzerland

³ANSTO LifeSciences, Australian Nuclear Science and Technology Organisation, Sydney, NSW, Australia

⁴Division of Geriatric Psychiatry, Department of Psychiatry, University Hospitals of Geneva, Geneva, Switzerland

⁵Department of Psychiatry, University of Geneva, Geneva, Switzerland

Corresponding author:

Philippe Millet, Division of Adult Psychiatry, University Hospitals of Geneva, Chemin du Petit Bel-Air, 2 1226 Geneva, Switzerland.
Email: Philippe.millet@hcuge.ch

information on the identity of the cells that produce TSPO. To reveal the cell origin of TSPO expression, several immunohistochemical (IHC) studies have been performed. Most of the studies demonstrate an involvement of microglia, which historically suggested that TSPO was a microglial marker.³ An astrocytic origin of TSPO has also been suggested.^{3,10,13,14} TSPO may also have an endothelial and neuronal origin.³ Thus, depending on the experimental approach, the authors show a variation in the number of cells expressing TSPO-immunoreactivity (TSPO-ir) without information on the quantity of TSPO per cell, or a variation of the intensity of TSPO-ir per unit area without information on the number of cells.^{15–17} Thus, these studies demonstrated the cellular origin of TSPO without precisely determining what these alterations stand for (alteration in the number of binding sites per cell or to an alteration of the number of cells expressing the binding sites).

Therefore, the existence of a variable cell origin of the TSPO greatly complicates the understanding of the SPECT/PET signal.³ In fact, the contribution of other cell types than microglia or astrocytes, such as endothelial cells and neurons, may have a confounding effect on *in vivo* imaging results,^{18,19} and it is difficult to know, in a given pathology, what is the contribution of each cell type in the PET/SPECT radioactive measures and what such a diversity may imply for the underlying biological significance of TSPO alterations. For instance, the cellular origin of the increase in TSPO signal demonstrated in PET studies in patients with AD^{7,20,21} or the decrease in TSPO in schizophrenia^{22–26} remains elusive.

To fill this gap, we have developed a new methodology coupling *in vivo* molecular imaging (in this study,

SPECT) to cell sorting performed by flow cytometry: fluorescence-activated cell sorting to radioligand-treated tissues (FACS–RTT). As a proof of concept, we used [¹²⁵I]CLINDE to quantify TSPO^{27,28} in a model of acute neuroinflammation induced by a unilateral stereotactic injection of lipopolysaccharide (LPS) or ciliary neurotrophic factor (CNTF). In our protocol, LPS is used to stimulate a microglial response,^{29,30} while the CNTF is used to stimulate both microglia and astrocytes.^{31–33} Two other groups of animals are studied: saline-injected rats to measure the impact of the surgery, and untreated rats to validate the reliability of the method by comparing the [¹²⁵I]CLINDE binding between left and right brain hemispheres. Then, we evaluated whether the FACS–RTT approach can be used in frozen human brain samples to quantify the cell origin of the TSPO binding, with AD as an example of pathology. Our general hypothesis is that the biological mechanisms underlying overexpression of TSPO may diverge depending on the type of neuroinflammation and the pathology.

Material and methods

Experimental design

The overall FACS–RTT procedure to assess the cellular origin of TSPO signal is shown in Figure 1. The animals were randomized in one of the three experimental conditions and received an injection into the left hippocampus of a solution containing either LPS, CNTF or saline (the groups were named accordingly). An additional group of rats (older animals) were used, to augment the chances of having a more robust and quantifiable TSPO signal, given that baseline TSPO expression increases with age³⁴ was also included.

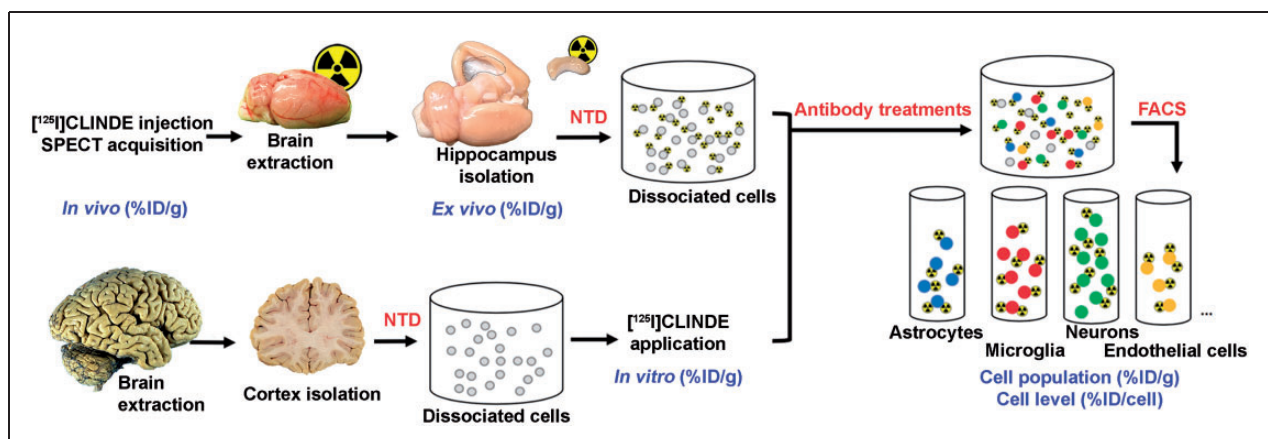


Figure 1. Overview of the fluorescence-activated cell sorting to radioligand-treated tissues (FACS–RTT) protocol. Schematic overview of the methodology used for the *in vivo*, *ex vivo*, *in vitro* and cellular measurement of the radioligand. %ID/cell: percentage of the injected dose/cell; %ID/g: percentage of the injected dose/g tissue weight; NTD: neural tissue dissociation.

The rats from the four groups underwent a SPECT exam with [125 I]CLINDE (in vivo determination of TSPO binding). At the end of the SPECT acquisition, hippocampi were extracted, measured in a gamma counter (ex vivo determination of TSPO binding) and processed for cell dissociation. Human brain samples were treated with [125 I]CLINDE following the cell dissociation procedure (in vitro determination of TSPO binding). All cells (in rat and human experiments) were then treated with the specific antibodies of the desired cell types (astrocytes, microglia, neurons and endothelial cells). The cells are then separated and counted with the FACS (including autofluorescent and negative cells, corresponding to unstained cells with the antibodies used). The radioactivity was finally measured in the different cell-sorted population (determination of TSPO binding at the cell population level), and the average radioactivity per cell was calculated (determination of TSPO binding at the cell unit level).

Animals

Sprague–Dawley rats (3 months old) and Fisher 344 rats (24 months old) were housed in light–dark cycle (LD 12:12) with food and water provided ad libitum. A random assignment of the Sprague–Dawley rats to the experimental groups was performed using unique identification numbers.³⁵ For the SPECT protocol followed by the FACS–RTT protocol, animals received stereotaxic injection of either LPS (n=7), CNTF (n=6) or saline (n=7). A radiotracer displacement FACS–RTT experiment was performed in a group of LPS-treated rats (n=3). For the comparison of the results of the SPECT and the FACS–RTT between left and right hippocampi in untreated rats, aged Fisher 344 rats (n=7) were used. All experimental procedures were conducted with the agreement of the Ethics Committee for Animal Experimentation of the Canton of Geneva and the General direction of health of the canton of Geneva, Switzerland. Data are reported in accordance with Animal Research: Reporting In Vivo Experiments (ARRIVE) guidelines.

Stereotaxic injections

Buprenorphine-treated (0.05 mg/kg s.c.) anesthetized (2% isoflurane) animals were mounted on a stereotaxic

apparatus. Three days before the imaging experiment, 2 μ l of LPS (5 μ g/ μ l), CNTF (2 μ g/ μ l) or saline was injected using a Hamilton syringe at the following coordinates relative to bregma: posterior, –5.6 mm; lateral, 5.0 mm and ventral, –5.0 mm. After injecting at a rate of 0.2 μ l/min, the syringe was left in place for 2 min before withdrawal.

Human brain samples

The human brain samples (n=9/group) were obtained from the Geneva Brain Bank³⁶ and were stored at –80 °C. Clinical variables of donors (age, gender, Braak stage and *Tspo* polymorphism status) are given in Table 1. A board-certified neuropathologist determined the Braak stage for neurofibrillary tangles. Frontal grey matter (100 mg) was dissected *ex temporally* for the FACS–RTT procedure. A second piece of tissue was used for genotyping, regarding the presence of the rs6971 polymorphism³⁷ within the TSPO gene (TaqMan SNP genotyping assay, Applied Biosystems). Subjects were classified as high affinity binders (HAB, absence of the rs6971 polymorphism), mixed affinity binders (MAB, heterozygous for this polymorphism) and low affinity binders (LAB, homozygous for the rs6971 polymorphism). LAB subjects were excluded from the analyses. The experimental procedure was approved by the Cantonal Commission for Research Ethics (CCER) of the Canton of Geneva and the General direction of health of the canton of Geneva, Switzerland.

[125 I]CLINDE synthesis

The CLINDE tributyltin precursor (100 μ g) in acid acetic (100 μ l) was incubated (70 °C, 20 min) with Na 125 I (5–10 mCi, PerkinElmer) and peracetic acid (37%, 5 μ l). After purification using a reversed-phase column, [125 I]CLINDE was concentrated using a Sep-Pak C18 cartridge in 95% acetonitrile (ACN). Then, ACN was evaporated, and [125 I]CLINDE was dissolved in saline.

SPECT scan acquisition and image processing

The 1-h in vivo imaging protocol began with the tail-vein injection of the [125 I]CLINDE (30.6 \pm 1.94 MBq) on anesthetized (2% isoflurane) animals placed in the

Table 1. Details of control and AD subjects.

Group	Braak stage	Age	HAB/MAB	Sex	PM delay (h)
Control	1.8 \pm 0.71	85.6 \pm 8.23	6/2	5m/3f	11.4 \pm 8.53
Alzheimer	5.2 \pm 0.67*	89.1 \pm 8.74	4/5	5m/4f	9.5 \pm 5.81

Mean \pm SD; *p < 0.001, two-tailed unpaired t test. PM: post mortem.

U-SPECT-II scan (miLabs, Utrecht, Netherlands). A dynamic SPECT acquisition (60×1 -min frames) was initiated upon injection of the radiotracer. SPECT images were reconstructed using a POSEM (0.4mm voxels, four iterations, six subsets) approach, and a radioactive decay correction was applied. A factor analysis denoising was applied on dynamic images, as previously described.^{38,39} The PMOD software (version 3.6; 2014, PMOD Technologies Ltd, Zurich, Switzerland) was used to process the images. Following a manual co-registration to the rat MRI implemented in the software, a volume-of-interest (VOI) template was used to extract the time-activity curves, as well as the radioactivity measurements corresponding to the time interval between the 45th and the 60th min post-injection.

Radioactivity measurements

Radioactive concentrations in rat and human brain extracts and in isolated cell types were measured on an automatic γ counting system.

Cell suspensions

Following a 1-h SPECT acquisition, animals were euthanized. For the effects of the radiotracer displacement procedure on FACS-RTT results, non-radioactive CLINDE (500 $\mu\text{g}/\text{kg}$) was injected 10 min after the [¹²⁵I]CLINDE injection, and rats were euthanized at 1-h after the [¹²⁵I]CLINDE injection (no SPECT scan was performed). The brain was quickly removed and dissected to isolate the left and right hippocampi. The tissues of the fresh rat were collected, and the frozen human samples were then prepared for FACS using the previously described protocol.⁴⁰ Briefly, mechanistic and enzymatic separation was applied to the tissues followed by a myelin depletion step. Cells were then suspended in buffer (0.1 M phosphate-buffered saline), 1 mM Ethylenediaminetetraacetic acid and 1% of Bovine Serum Albumin) and treated with APC anti-rat CD11b (1/800; Biolegend), FITC anti-rat CD90 (1/250; Biolegend), PE-Cy7 anti-rat CD31 (1/100; Invitrogen) and rabbit anti-GLT1 (1/100; Novus) antibodies for rat samples and with BV 421 anti-human CD45 (1/800; BD Horizon), PE-Cy7 anti-human CD31 (1/100; Invitrogen) and rabbit anti-GLT1 (1/100; Novus) antibodies for human samples. After 20 min of incubation and washing, a secondary antibody (PE goat anti-rabbit; 1/500; Life technologies) was applied for 15 min. Then, cells were suspended in 250 μl of the buffer. An additional step was performed for human samples: before the addition of antibodies, cells were treated with [¹²⁵I]CLINDE for 15 min, followed by a washing step.

Fluorescence-activated cell sorting

Dead rat cells were excluded using a DAPI staining during data collection. Unstained and single stain cells (from both human and rat samples) were used to identify positive and negative cells for each antibody, to identify autofluorescent cells, to determine the values of compensation (to correct for the interferences between fluorochromes), to validate the functioning of each antibody and to draw the gate of cell sorting for each antibody. Firstly, cells were sorted based on their forward and side scatter from all possible events. Single cells were then sorted based on their autofluorescence, and their fluorescence considering PE-GLT1 positive cells and PE-Cy7-Pecam/CD31 positive cells. Negative cells were then sorted based on their fluorescence considering FITC-CD90 positive cells and either APC-CD11b positive cells (rat samples) or BV-CD45 positive cells (human samples). Cells that are neither autofluorescent nor stained with any of the antibodies are sorted and expressed as negative cells. The cell number was determined for each cell population during data collection (Beckman Coulter MoFlo Astrios).

Western blot

To further validate the purity of the glial cells that were sorted with FACS, western blot experiments were performed. Following cell sorting, CD11b⁺, GLT1⁺, CD31⁺ and CD90⁺ cells were lysed in extraction buffer (50 mM Tris (pH 7.4), 150 mM NaCl, 0.02% sodium azide, 0.1% SDS, 1% Nonidet P-40, 12 mM sodium deoxycholate, 1x proteinase inhibitor). Protein homogenates were treated with 5% β -mercaptoethanol in 1x LDS (Invitrogen) and separated using 12% NuPAGE Tris-Acetate gels (Invitrogen). After transfer to nitrocellulose membrane, proteins were treated with mouse anti-Gfap (1/500; Invitrogen) or rabbit anti-Iba1 (1/500; Wako) for 48 h in 0.2% Tween 20, 5% milk and 1x PBS buffer. Secondary antibodies (rabbit anti-mouse and goat anti-rabbit, 1/1000) were incubated for 1 h. Twice washing (20 min, 0.2% Tween 20, 5% milk, 1x PBS buffer) was performed after incubation with antibodies. Bands were detected with the chemiluminescent ECL detection system (Amersham).

Statistical analyses

Radioactivity was expressed as a percentage of the injected dose/g tissue weight (%ID/g) or as a percentage of the injected dose/cell (%ID/cell). Cell isolation and FACS procedures were performed at blind conditions. Statistical analyses were performed using the two-way analyses of variance (ANOVA) with cell type and groups as between-subject variables.

When the group \times cell type interaction was significant, comparisons were performed using paired (rat samples) or unpaired (human samples) two-tailed Student's *t*-tests. No adjustment for multiple comparisons was made since we used a planned comparison including only the difference between groups and not the entire contrasts (six pairs out of the 66 total pairs). All analyses were performed using Statistica software (Statistica 8.0; StatSoft). Data are presented as mean \pm SD. A sample size analysis with the graphical Douglas Altman's nomogram approach⁴¹ was performed, and significant data was only reported if $p \leq 0.05$ and $\beta < 0.2$.

Results

[¹²⁵I]CLINDE representative SPECT images are presented in Figure 2. In animals having received unilateral LPS and CNTF injections (Figure 2(a) and (b), respectively), an increase in the [¹²⁵I]CLINDE binding is observed. In animals having received a saline injection, as well as in the control group of aged animals having received no treatment, no left/right difference is observed (Figure 2(c) and (d), respectively). Following the SPECT experiment, hippocampi were processed for the dissociation procedure. Figure 3(a) and (b) shows the result of a representative cell-sorting experiment

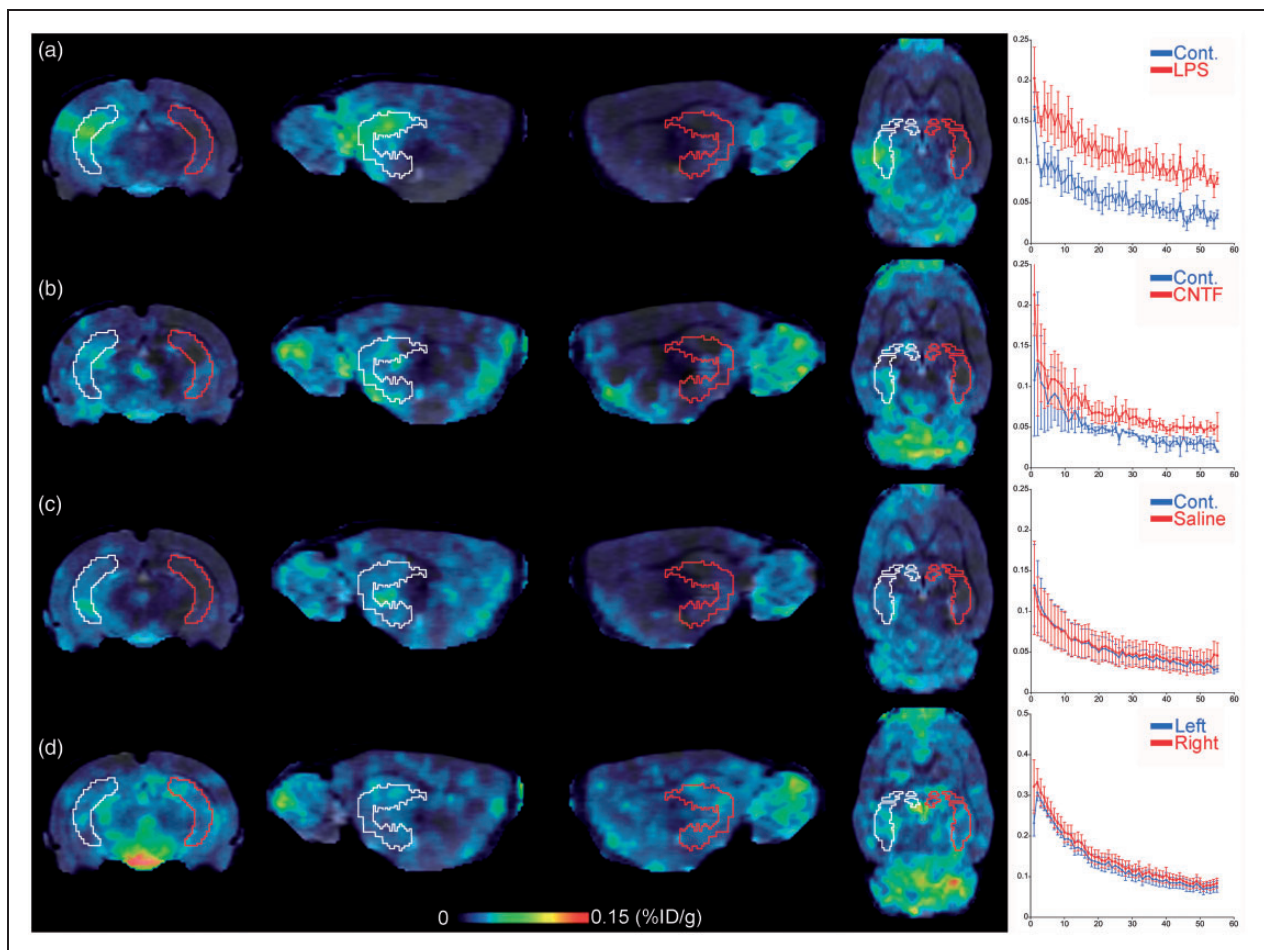


Figure 2. TSPO brain imaging using SPECT with [¹²⁵I]CLINDE. Representative images of the SPECT TSPO signal at the level of the hippocampus in the ipsilateral (volume-of-interest drawn in white) and the contralateral (volume-of-interest drawn in red) side of the injection of LPS (a), CNTF (b), Saline (c) as well as in untreated rats (d). Images (corresponding to the 45–60 min post-injection) were coregistered to the MRI atlas in the coronal (left), sagittal (center), and horizontal (right) planes. The in vivo time–activity-curves obtained in the ipsilateral and the contralateral side of the injection are presented on the right of the images. SPECT: single-photon emission computed tomography; TSPO: translocator protein; LPS: lipopolysaccharide; CNTF: ciliary neurotrophic factor.

with the gate of cell sorting for each antibody. No difference in the median fluorescent intensity (MFI) was observed between left and right hippocampi, and between the AD and control tissues, whatever the antibody used (not shown). A western blot confirmation of the identity of the GLT1⁺ and CD11b⁺ cells was performed (Figure 3(c)). GFAP is only observed in cells sorted using the GLT1-specific antibody, and IBA1 is only observed in cells sorted using the CD11b antibody. The quantification of TSPO binding in the different experiments and in the various cell types is described in detail below.

Cell origin of LPS-induced TSPO overexpression

LPS induced a significant increase in TSPO binding that is observed both *in vivo* and *ex vivo* ($p < 0.01$, Figure 4(a) and (b)). The injection of LPS increased the radioactive signal in the microglial cell population (Figure 4(c), $p < 0.001$) without any increase in the number of TSPO binding sites per microglial cell (Figure 4(d)) but with an increase in the number of microglial cells (Figure 4(e), $p < 0.001$). We did not observe any alterations on the other cell types (see Figure 4(c) to (e) for astrocytes, endothelial cells and neurons and Supplemental Figure 1 for autofluorescent and negative cells, that are, negative for all the used antibodies).

To validate the specificity of the increase in the [¹²⁵I]CLINDE, an additional group of LPS-treated rats received a co-injection of both radioactive and non-radioactive CLINDE. The co-injection of both radioactive and non-radioactive CLINDE abolished the left/right difference of TSPO binding as measured: (a) at the *ex vivo* level (left/right difference: LPS group, 2.92 ± 0.43 ; LPS + non-radioactive CLINDE group, 1.27 ± 0.1) and (b) at the microglial cell population level (left/right difference: LPS group, 10.4 ± 3.11 ; LPS + non-radioactive CLINDE group, 1.28 ± 1.21).

Cell origin of CNTF-induced TSPO overexpression

Figure 4(f) to (g) shows the left/right difference in TSPO binding induced by CNTF as measured at *in vivo* ($p < 0.05$) and *ex vivo* ($p < 0.05$) levels. The results of the FACS-RTT protocol indicated that the injection of CNTF increased the radioactivity levels due to microglia at both the cell population level ($p < 0.05$, Figure 4(h)) and the cell level ($p < 0.01$, Figure 4(i)) without any change in number of cells (Figure 4(j)). CNTF also stimulated the TSPO signal in the astrocytic cell population ($p < 0.05$, Figure 4(h)). CNTF did not induce any alterations on the other cell types (see Figure 4(c) to (e) for endothelial cells and neurons, and Supplemental Figure 1 for autofluorescent and negative cells).

Absence of TSPO overexpression in response to a saline injection

To validate the specificity of the effects of LPS and CNTF in term of TSPO overexpression, an additional group of rats received a sham unilateral injection (i.e. saline). Such an injection did not induce any difference between the left and the right hippocampus (Figure 5(a) and (b), *in vivo* and *ex vivo*). Saline did not modify neither the TSPO from astrocytes, microglia, neurons and endothelial cells nor the number of cells sorted (Figure 5(c) to (e)). The only statistical difference observed is an unexpected increase in the [¹²⁵I]CLINDE signal due to autofluorescent cells (Supplemental Figure 2).

Absence of left/right difference in TSPO binding in the hippocampus of untreated rats

To underline the absence of endogenous left/right differences in the [¹²⁵I]CLINDE binding in the hippocampus, we used aged rats to potentialize the TSPO detection, as TSPO was previously shown to increase with age in both human and rodents.^{4,6,34,42–44} The comparison of the left and the right hippocampus of untreated rats did not find any statistically significant difference (Figure 5(f) to (j), Supplemental Figure 2).

Cell origin of TSPO overexpression in human: the example of Alzheimer's disease

The results of the comparison of TSPO binding in the frontal cortex between a group of AD patients and age- and sex-matched controls (details on the population is indicated in Table 1) are presented in the Figure 6. The genotyping revealed that 10 subjects were HAB and seven were MAB. Only one subject was LAB and excluded from the study. At the overall cell population level, no difference was observed between groups (Figure 6(a)). In marked contrast, the FACS-RTT protocol permitted to identify an increase in the radioligand uptake in AD in microglia ($p < 0.05$), astrocytes ($p < 0.05$) (Figure 6(b)) as well as a significant proliferation of microglial cells ($p < 0.05$, Figure 6(d)). No difference was shown in the number of TSPO binding sites per cell (Figure 6(c)). The autofluorescent cell population showed an increase in their cell number ($p < 0.05$, Supplemental Figure 3).

Discussion

To our knowledge, this study is the first to describe the quantification of the *in vivo* binding of a radiotracer at the cell-population level. This new method, FACS-RTT, allowed us to highlight two different types of

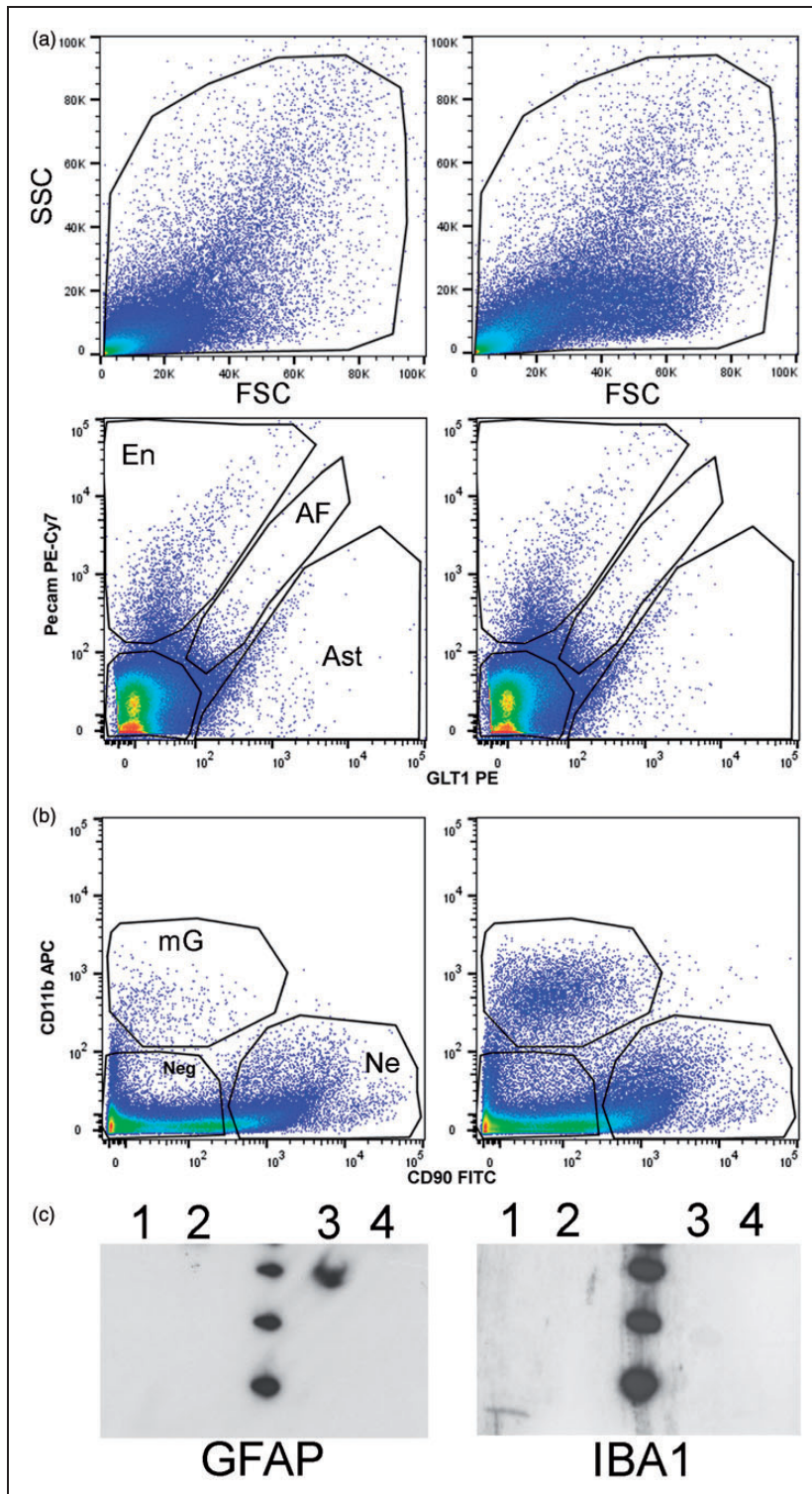


Figure 3. Example of cell sorting. (a) Representative images of the alive cell population depending on size (forward scatter, FSC) and granulometry (side scatter, SSC) in the LPS-injected side (right panel) and the contralateral (left panel) side. (b) Representative images of cell sorting, as a function of GLT1-PE, Pecam PE-Cy7, CD11b APC and CD90 FITC, in the LPS (right panel) and the contralateral (left panel) side of the injection. (c) Representative immunoblots validating the astrocytic and microglial identity of the GLT1 and CD11b positive cells, respectively. Immunoblots were performed on sorted cells (lane 1: CD11b⁺; lane 2: CD90⁺; lane 3: GLT1⁺ and lane 4: CD31⁺) and exposed to antibody directed against either GFAP (left) or IBA1 (right). GFAP is only observed in GLT1 positive cells and IBA1 is only observed in CD11b positive cells. The molecular weight (at the center of blots) indicates bands around 20, 30 and 40 kDa. AF: autofluorescent; Ast: astrocyte (GLT1 positive cells and negative for all other markers); En: endothelial (Pecam positive cells and negative for all other markers); mG: microglia (CD11b positive cells and negative for all other markers); Ne: neuron (CD90 positive cells and negative for all other markers); Neg: cells negative for all markers.

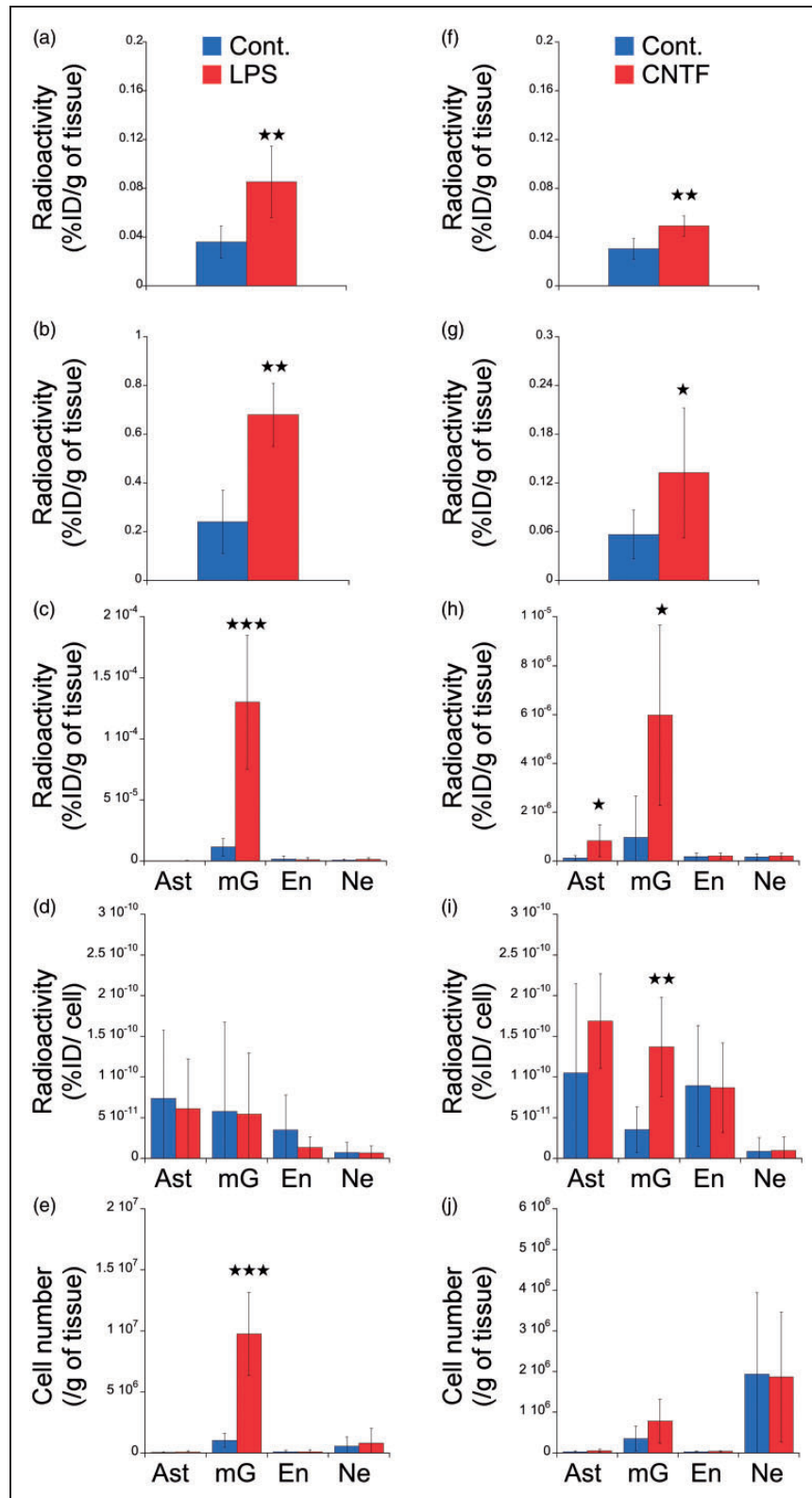


Figure 4. Cell origin identification of TSPO overexpression in response to unilateral brain injection of LPS or CNTF. Animals received either LPS (a to e) or CNTF (f to j). The radioactivity (%injected dose /g of tissue, %ID/g) was measured in vivo (a and f), ex vivo (b and g) and in each cell population (c and h) in the ipsilateral (red) and the contralateral (blue) side of the injection. (d and i) Radioactivity per cell (%injected dose/cell) in each cell population in the ipsilateral (red) and the contralateral (blue) side of the injection. (e and j) number of cells sorted in the ipsilateral (red) and the contralateral (blue) side of the injection. Ast: astrocyte (GLT1 positive cells and negative for all other markers); Cont.: contralateral; CNTF: ciliary neurotrophic factor; En: endothelial (Pecam positive cells and negative for all other markers); LPS: lipopolysaccharide; mG: microglia (CD11b positive cells and negative for all other markers); Ne: neuron (CD90 positive cells and negative for all other markers).

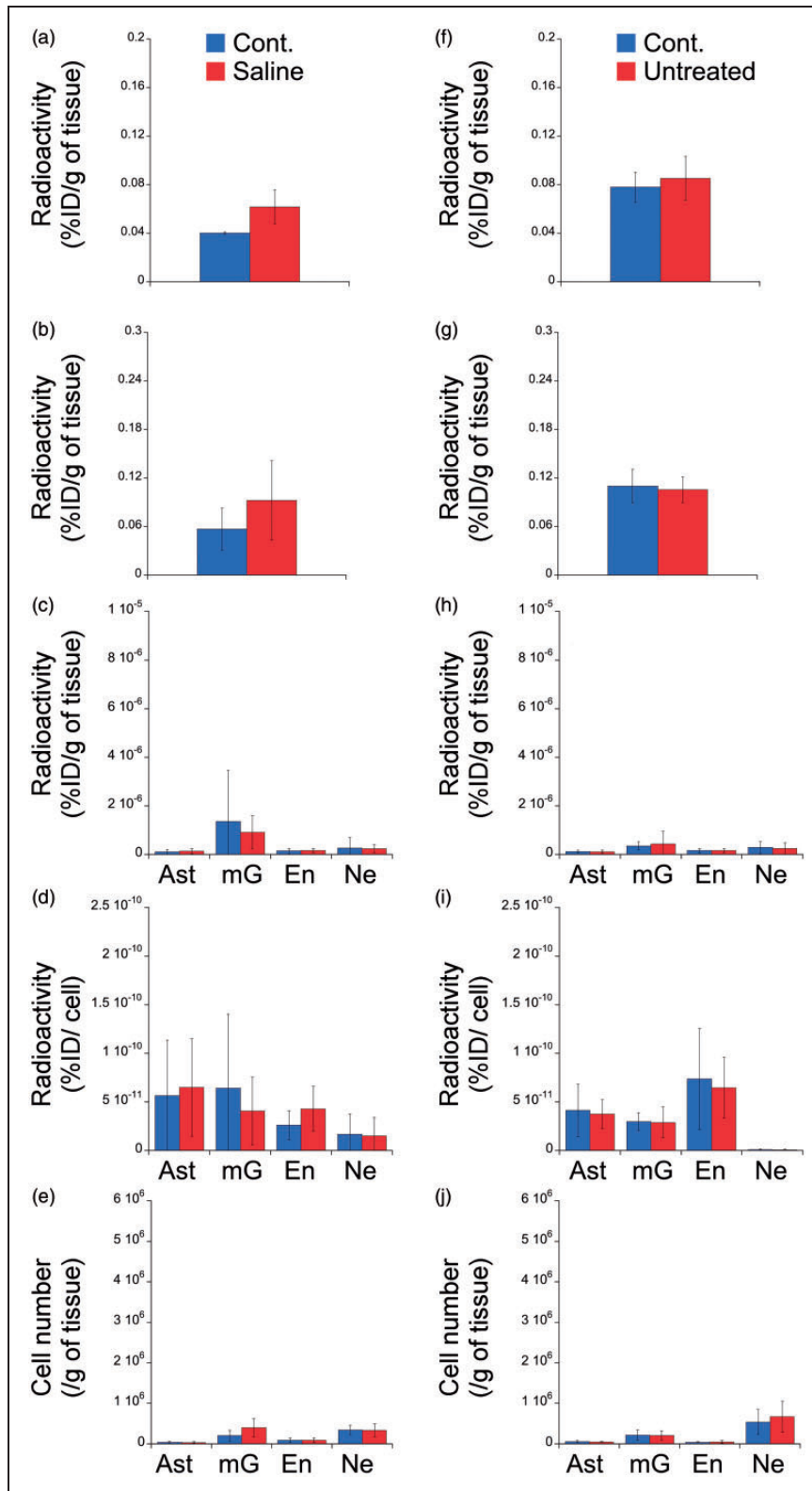


Figure 5. Cell origin identification of TSPO expression in response to unilateral brain injection of Saline and in untreated rats. Animals received saline (a to e) or were untreated (f to j). The radioactivity (%injected dose/g of tissue, %ID/g) was measured in vivo (a and f), ex vivo (b and g) and in each cell population (c and h) in the ipsilateral (red) and the contralateral (blue) side of the injection. (d and i) Radioactivity per cell (%injected dose/cell) in each cell population in the ipsilateral (red) and the contralateral (blue) side of the injection. (e and j) number of cells sorted in the ipsilateral (red) and the contralateral (blue) side of the injection. Ast: astrocyte (GLT1 positive cells and negative for all other markers); Cont.: contralateral; En: endothelial (Pecam positive cells and negative for all other markers); mG: microglia (CD11b positive cells and negative for all other markers); Ne: neuron (CD90 positive cells and negative for all other markers).

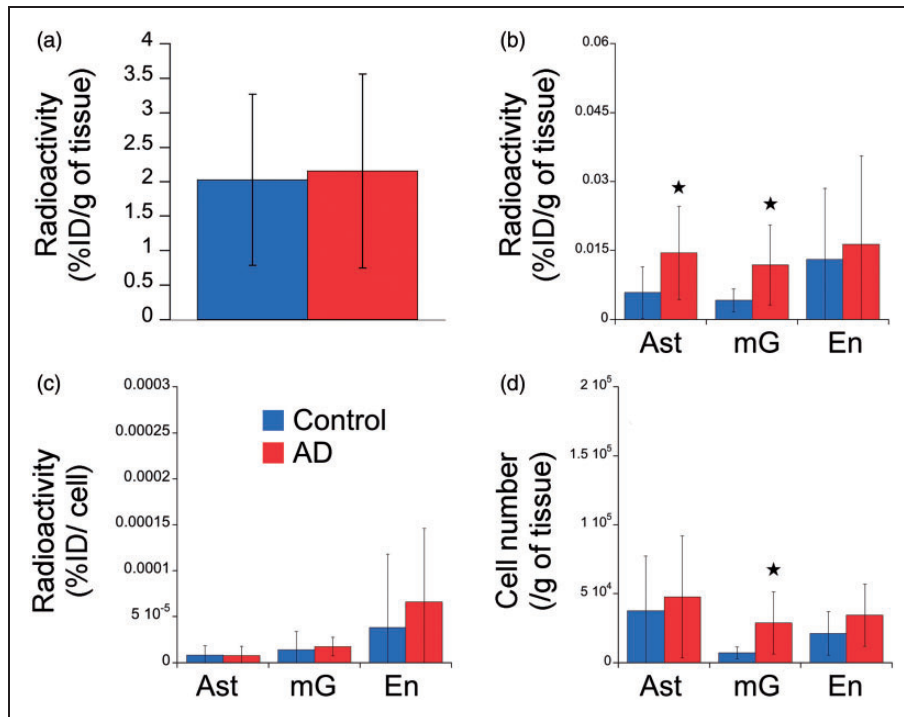


Figure 6. Determination of the cell origin of TSPO overexpression in frontal cortex of Alzheimer's disease. (a) In vitro radioactivity (%injected dose /g of tissue, %ID/g) in the frontal cortex of control (blue) and AD (red) subjects. (b) Radioactivity (%injected dose /g of tissue) in each cell population in control (blue) and AD (red) subjects. (c) Radioactivity per cell (%injected dose /cell) in the cell population in control (blue) and AD (red) subjects. (d) Number of cells in control (blue) and AD (red) subjects. AD: Alzheimer's disease; Ast: astrocyte (GLT1 positive cells and negative for all other markers); En: endothelial (CD31 positive cells and negative for all other markers); mG: microglia (CD45 positive cells and negative for all other markers).

TSPO-dependent neuroinflammation in response to an intracerebral injection of LPS and CNTF. In the first case, the in vivo observed increase in TSPO binding was attributed to an increase in the number of microglial cells and thus to an increase in TSPO binding in the microglial population. In contrast, in response to the CNTF, an increase in the binding of TSPO in both astrocyte and microglial cell populations is detected with a significant increase in the number of binding sites per microglial cell, without any expansion of the number of cells. Our methodology was then applied to samples of human cortex, which corresponds to a radioligand binding assay coupled to the FACS. With Alzheimer's pathology as an example, we show an increase in the TSPO signal is of astrocytic and microglial origin, with an increase in the number of microglial cells.

In vivo molecular imaging approaches cannot identify the cellular origin and the cellular mechanisms of adaptation (variation in the number of targets per cell and/or in the number of cells). In the case of TSPO, the multi-cellular origin represents a challenge for the quantification using in vivo imaging. Firstly, microglia and astrocytes have distinct roles in brain physiology

and pathophysiology. It is thus important to know whether a given alteration in the TSPO binding measured in vivo is of microglial or astrocytic origin to better understand the underlying inflammatory process, its functional consequences and the implications for the development of therapeutic approaches. In that idea, we showed that although the in vivo signal in response to LPS and CNTF is similar (i.e. increase in TSPO binding), the identity of the cells and the underlying mechanisms that account for this TSPO overexpression are different, much probably representing distinct biological processes. The distinction between TSPO from the astrocytes and that of microglia will better characterize the pathophysiological mechanisms involved in human physiology and pathology with a more precise approach, which is complementary to in vivo imaging. Secondly, deciphering the contribution of endothelial cells to the increase of TSPO binding in a given pathology is a major challenge in the field¹⁹: the need to separately model the endothelial binding, in order to isolate its contribution from the glial binding in the kinetic analysis of TSPO brain imaging studies is debated. With the FACS-RTT approach introduced here, we identify the differential origin of the increase

in TSPO binding depending on the experimental paradigm of the induction of the inflammation.

To validate the specificity of the responses, we used a sham-injection group to evaluate the impact of the surgery and of the injection per se. In saline-injected rats, we show the lack of response in terms of TSPO binding and of cell number. Thus, the present study demonstrates a segregation between microglial and astrocytic reactivity in response to LPS and CNTF with respect to TSPO overexpression. This observation is important as it makes it possible to demonstrate that TSPO is not only a marker of microglial activation, it can mark variations at the astrocyte level and alterations in the number of targets per cell. Fluorescent immunohistochemistry is qualitative in nature and does not allow this level of quantitative precision, but in agreement with our data, it has been shown that TSPO is expressed by all the above-mentioned cells.^{10,18,45} We cannot exclude that a part of the TSPO signal in Cd11b⁺ cells is coming from a possible LPS-induced infiltration of circulating monocytes/macrophages but this is out of the scope of the present article. Further studies with an optimized choice of antibodies may answer this potentially important question.

In vitro FACS–RTT in human samples was restricted to astrocytes, microglial and endothelial cells^{19,46–48} as it was previously shown that the expression of TSPO in human AD brain did not involve neurons.⁴⁷ At the whole-tissue level, we did not show any difference between AD and control but, interestingly, the increase of TSPO between control tissue and AD becomes significant when the TSPO binding is measured individually in each cell type. The validity of the finding that TSPO increase in AD is of astrocytic and microglial origin is further supported by the relevant literature implicating the activation of microglia and astrocytes in AD.^{49–51} Other cell types, notably endothelial cells, contribute to the overall [¹²⁵I]CLINDE signal but not to the signal increase in AD patients. This finding may have major implications for in vivo clinical PET and SPECT imaging of neuroinflammation in AD. Using the FACS–RTT approach, the origin of the increase in TSPO binding observed in AD patients is found to be essentially glial. This finding, if extended to other brain areas, suggests that a separate modelling of the endothelial binding may be unnecessary in clinical studies of TSPO in AD. Overall, such a translational approach may enhance the understanding of TSPO-related neuroinflammation in AD and potentially in other brain pathologies, from both a diagnostic and therapeutic perspective.

In this study, we describe the use of a new method, complementary to in vivo imaging. In order to provide arguments for the validation of the FACS–RTT techniques, we have made various observations: (i) In

untreated animals, we show the absence of left/right difference for the number of cells, the TSPO binding per cell and the TSPO binding per cell population. This brings an argument on the reliability of the repeatability of the procedure. A true test–retest (i.e. repetition of the whole procedure) cannot be performed since the cell separation protocol is a ‘terminal’ procedure, and the dissociated cells cannot be used for multiple FACS experiments. As the left and right hippocampi are separately treated (in terms of cell dissociation and FACS), they can represent an index of repeatability. (ii) On sorted cell populations using previously validated antibodies,⁴⁰ we show that only the GLT1⁺ population is GFAP⁺ and that only the CD11b⁺ population is IBA1⁺, which is an index of purity of the sorted cells. (iii) In response to LPS, we show an increase in the number of microglial cells, which agrees with the literature.^{30,52} In the cortex of AD patients, we also show this cell expansion of microglia, which confirms the previous IHC data.^{53,54} (iv) We did not report alteration in the number of astrocytes in the cortex of AD patients, which corroborates previous IHC observations.^{55–57} (v) In response to CNTF, we reported an activation of both microglia and astrocytes which is in accordance with previous literature.^{31–33} (vi) The co-injection of radioactive and non-radioactive CLINDE results in an absence of radioactive signal at the cellular level which proves that the CLINDE–TSPO binding remains specific even after the FACS procedure. Thus, our observations and the relevant literature come together to validate our approach. In addition, the FACS–RTT approach can identify the mechanisms of TSPO alterations in the cell population (i.e. number of target/cell and number of cells) that is not possible in IHC.^{10,15–17} By contrast, IHC allows to maintain the cellular architecture and thus to determine cell–cell interactions. Therefore, IHC and FACS–RTT approaches are, to our view, complementary.

By analogy with the single cell RT–qPCR after FACS for the RNAs quantification, the FACS–RTT seems a valid technique for the single cell radioligand detection of target proteins. As in our human samples experiment, the data at the cellular level may be different from this at the tissue level. Therefore, the FACS–RTT appears to be complementary to in vivo imaging and contribute a level of precision that is impossible to obtain in in vivo or ex vivo imaging. In our study, the various models of acute neuroinflammation did not have any impact on the endothelial TSPO. This observation does not exclude the presence of alterations of the endothelial TSPO in other brain pathologies, and the FACS–RTT approach should be very useful in this context. We have shown the cellular origin of TSPO increases in the LPS- and CNTF-treated groups as well as in the human frontal cortex in AD.

FACS–RTT may also be used to gain in-depth understanding of the mechanism of alterations in TSPO binding in other brain pathologies, even when a decrease in its binding is detected in in vivo imaging, as in schizophrenia.²⁶ In this example, FACS–RTT could be used to better understand in which cells the TSPO binding is decreased and/or if the number of cells that express TSPO is modified in post mortem samples from schizophrenic patients (and even animal models). The limiting factor is the possibility of detecting TSPO, which is why in our study we used older animals as controls to potentiate the detection of TSPO. The applicability of FACS–RTT is not limited to [¹²⁵I]CLINDE. It can be used not only with all others TSPO tracers (provided that the radioisotope used has half-lives compatible with the duration of the procedure) but also with all radioligands that present binding in multiple cell types. This is the case, for example, of the expression of many neurotransmitter receptors (such as dopamine and acetylcholine receptors).^{58–61} Overall, the potential of our technique is considerable.

One of the limitations of the present study arises from the presence of autofluorescent cells in elderly subjects and patients as well as in older animals. Residues of lysosomal digestion, called lipofuscin, are fluorescent and are known to accumulate with ageing in neurons, microglia and astrocytes. The cell origin of autofluorescent cells cannot be identified by FACS. Thus, our data are based on the identification of non-autofluorescent positive cells. We excluded double positive cells (for one of the antibodies and autofluorescence). The second limitation of our study is the lack of possible comparison between the different sorted cell types. Indeed, the efficacy of the antibodies to capture the targeted cells and the accuracy of the cell sorting as a function of the wavelength and the light intensity of the antibodies differs across cell types. Thus, direct comparisons between the alterations in TSPO binding between different cell types are limited. An optimization of the antibodies is warranted to improve the accuracy of the results.

We conclude that the origin of an increase in TSPO probably depends on the type of neuroinflammation and should not be generalized across brain pathologies. Future clinical studies should therefore be informed by preclinical animal models or post mortem human brain tissue studies to take into consideration the cell types involved in the alterations of TSPO observed in in vivo molecular imaging, as well as the direction of the changes. Overall, the methodology proposed here can distinguish the cell types (astrocytes, microglia, neurons, etc.) involved in the uptake of a radioligand in the CNS both regarding the binding of the radioligand in each cell type as well as the alterations in the number of cells in which this uptake is observed.

This methodology presents a major interest in the field of in vivo molecular imaging as it may provide unprecedented insight into the cellular underpinnings of radioligand binding in the CNS. Thus, the FACS–RTT techniques appear as a complementary approach to in vivo imaging and to immuno-fluorescence imaging to decipher the cellular origin of radioligand binding changes.

Funding

The author(s) received no financial support for the research, authorship, and/or publication of this article.

Acknowledgements

We are grateful to Maria Surini, Marouane Ben Ammar and Jean-Pierre Aubry-Lachainaye for technical assistance. ST received support from the ‘Maria Zaousi’ Memorial Foundation through the Greek State Scholarship Foundation and the Jean and Madeleine Vachoux Foundation; BBT and KC were supported by the Velux foundation (project no. 1193). This work was supported by the Swiss National Science Foundation (no. 320030-184713).

Declaration of conflicting interests

The author(s) declared no potential conflicts of interest with respect to the research, authorship, and/or publication of this article.

Authors’ contributions

BBT, ST and PM designed the experiment. BBT, KC and ZM performed the experiment. EK provided the human samples; BHF and MCG provided the CLINDE precursor. BBT, ST, KC and PM analyzed and interpreted the data. BBT, ST and PM wrote the article and KC, ZM, EK, BHF and MCG revised it.

Supplemental material

Supplemental material for this paper can be found at the journal website: <http://journals.sagepub.com/home/jcb>

ORCID iDs

Benjamin B Tournier  <https://orcid.org/0000-0002-8027-7530>

Zadith Medina  <https://orcid.org/0000-0002-7304-7403>

References

1. Chaney A, Williams SR and Boutin H. In vivo molecular imaging of neuroinflammation in Alzheimer’s disease. *J Neurochem* 2019; 149: 438–451.
2. Rupprecht R, Papadopoulos V, Rammes G, et al. Translocator protein (18 kDa) (TSPO) as a therapeutic target for neurological and psychiatric disorders. *Nat Rev Drug Discov* 2010; 9: 971–988. 2010/12/02.
3. Guilarte TR. TSPO in diverse CNS pathologies and psychiatric disease: a critical review and a way forward. *Pharmacol Ther* 2019; 196: 44–58.

4. Cagnin A, Brooks DJ, Kennedy AM, et al. In-vivo measurement of activated microglia in dementia. *Lancet* 2001; 358: 461–467.
5. Golla SS, Boellaard R, Oikonen V, et al. Quantification of [18F]DPA-714 binding in the human brain: initial studies in healthy controls and Alzheimer's disease patients. *J Cereb Blood Flow Metab* 2015; 35: 766–772.
6. Gulyas B, Vas A, Toth M, et al. Age and disease related changes in the translocator protein (TSPO) system in the human brain: positron emission tomography measurements with [11C]vinpocetine. *Neuroimage* 2011; 56: 1111–1121.
7. Hamelin L, Lagarde J, Dorothee G, et al. Early and protective microglial activation in Alzheimer's disease: a prospective study using 18F-DPA-714 PET imaging. *Brain* 2016; 139: 1252–1264.
8. Maeda J, Zhang MR, Okauchi T, et al. In vivo positron emission tomographic imaging of glial responses to amyloid-beta and tau pathologies in mouse models of Alzheimer's disease and related disorders. *J Neurosci* 2011; 31: 4720–4730.
9. Rapic S, Backes H, Viel T, et al. Imaging microglial activation and glucose consumption in a mouse model of Alzheimer's disease. *Neurobiol Aging* 2013; 34: 351–354.
10. Tournier BB, Tsartsalis S, Rigaud D, et al. TSPO and amyloid deposits in sub-regions of the hippocampus in the 3xTgAD mouse model of Alzheimer's disease. *Neurobiol Dis* 2019; 121: 95–105. 2018/09/28.
11. Kreisl WC, Lyoo CH, McGwier M, et al. In vivo radioligand binding to translocator protein correlates with severity of Alzheimer's disease. *Brain* 2013; 136: 2228–2238.
12. Frey KA and Albin RL. Receptor binding techniques. *Curr Protoc Neurosci* 2001. Chapter 1: Unit1 4. 2008/04/23.
13. Ji B, Maeda J, Sawada M, et al. Imaging of peripheral benzodiazepine receptor expression as biomarkers of detrimental versus beneficial glial responses in mouse models of Alzheimer's and other CNS pathologies. *J Neurosci* 2008; 28: 12255–12267.
14. Venneti S, Lopresti BJ, Wang G, et al. PK11195 labels activated microglia in Alzheimer's disease and in vivo in a mouse model using PET. *Neurobiol Aging* 2009; 30: 1217–1226.
15. Hannestad J, Gallezot JD, Schafsbauer T, et al. Endotoxin-induced systemic inflammation activates microglia: [(1)1C]PBR28 positron emission tomography in nonhuman primates. *Neuroimage* 2012; 63: 232–239.
16. Toth M, Little P, Arnberg F, et al. Acute neuroinflammation in a clinically relevant focal cortical ischemic stroke model in rat: longitudinal positron emission tomography and immunofluorescent tracking. *Brain Struct Funct* 2016; 221: 1279–1290.
17. Notter T, Coughlin JM, Gschwind T, et al. Translational evaluation of translocator protein as a marker of neuroinflammation in schizophrenia. *Mol Psychiatry* 2018; 23: 323–334.
18. Rizzo G, Veronese M, Tonietto M, et al. Kinetic modeling without accounting for the vascular component impairs the quantification of [(11)C]PBR28 brain PET data. *J Cereb Blood Flow Metab* 2014; 34: 1060–1069.
19. Veronese M, Reis Marques T, Bloomfield PS, et al. Kinetic modelling of [(11)C]PBR28 for 18 kDa translocator protein PET data: a validation study of vascular modelling in the brain using XBD173 and tissue analysis. *J Cereb Blood Flow Metab* 2017. 271678X17712388. DOI: 10.1177/0271678X17712388.
20. Varrone A, Mattsson P, Forsberg A, et al. In vivo imaging of the 18-kDa translocator protein (TSPO) with [18F]FEDAA1106 and PET does not show increased binding in Alzheimer's disease patients. *Eur J Nucl Med Mol Imaging* 2013; 40: 921–931.
21. Versijpt JJ, Dumont F, Van Laere KJ, et al. Assessment of neuroinflammation and microglial activation in Alzheimer's disease with radiolabelled PK11195 and single photon emission computed tomography. A pilot study. *Eur Neurol* 2003; 50: 39–47.
22. Bloomfield PS, Selvaraj S, Veronese M, et al. Microglial activity in people at ultra high risk of psychosis and in schizophrenia: an [(11)C]PBR28 PET brain imaging study. *Am J Psychiatry* 2016; 173: 44–52.
23. Collste K, Plaven-Sigray P, Fatouros-Bergman H, et al. Lower levels of the glial cell marker TSPO in drug-naive first-episode psychosis patients as measured using PET and [11C]PBR28. *Mol Psychiatry* 2017. DOI: 10.1038/mp.2016.247.
24. De Picker LJ, Morrens M, Chance SA, et al. Microglia and brain plasticity in acute psychosis and schizophrenia illness course: a meta-review. *Front Psychiatry* 2017; 8: 238.
25. Hafizi S, Tseng HH, Rao N, et al. Imaging microglial activation in untreated first-episode psychosis: a PET study with [18F]FEPPA. *Am J Psychiatry* 2017; 174: 118–124.
26. Plaven-Sigray P, Matheson GJ, Collste K, et al. Positron emission tomography studies of the glial cell marker translocator protein in patients with psychosis: a meta-analysis using individual participant data. *Biol Psychiatry* 2018; 84: 433–442.
27. Arlicot N, Katsifis A, Garreau L, et al. Evaluation of CLINDE as potent translocator protein (18 kDa) SPECT radiotracer reflecting the degree of neuroinflammation in a rat model of microglial activation. *Eur J Nucl Med Mol Imaging* 2008; 35: 2203–2211. 2008/06/10.
28. Tsartsalis S, Dumas N, Tournier BB, et al. SPECT imaging of glioma with radioiodinated CLINDE: evidence from a mouse GL26 glioma model. *EJNMMI Res* 2015; 5: 9.
29. Norden DM, Trojanowski PJ, Villanueva E, et al. Sequential activation of microglia and astrocyte cytokine expression precedes increased Iba-1 or GFAP immunoreactivity following systemic immune challenge. *Glia* 2016; 64: 300–316.
30. Furube E, Kawai S, Inagaki H, et al. Brain region-dependent heterogeneity and dose-dependent difference in transient microglia population increase during lipopolysaccharide-induced inflammation. *Sci Rep* 2018; 8: 2203.

31. Levison SW, Ducceschi MH, Young GM, et al. Acute exposure to CNTF in vivo induces multiple components of reactive gliosis. *Exp Neurol* 1996; 141: 256–268.
32. Krady JK, Lin HW, Liberto CM, et al. Ciliary neurotrophic factor and interleukin-6 differentially activate microglia. *J Neurosci Res* 2008; 86: 1538–1547.
33. Lin HW, Jain MR, Li H, et al. Ciliary neurotrophic factor (CNTF) plus soluble CNTF receptor alpha increases cyclooxygenase-2 expression, PGE2 release and interferon-gamma-induced CD40 in murine microglia. *J Neuroinflammation* 2009; 6: 7.
34. Kumar A, Muzik O, Shandal V, et al. Evaluation of age-related changes in translocator protein (TSPO) in human brain using (11)C-[R]-PK11195 PET. *J Neuroinflammation* 2012; 9: 232.
35. Johnson PD and Besselsen DG. Practical aspects of experimental design in animal research. *ILAR J* 2002; 43: 202–206.
36. Kovari E, Hof PR and Bouras C. The Geneva brain collection. *Ann N Y Acad Sci* 2011; 1225(Suppl 1): E131–E146.
37. Owen DR, Gunn RN, Rabiner EA, et al. Mixed-affinity binding in humans with 18-kDa translocator protein ligands. *J Nucl Med* 2011; 52: 24–32.
38. Tsartsalis S, Moulin-Sallanon M, Dumas N, et al. Quantification of GABAA receptors in the rat brain with [(123)I]Iomazenil SPECT from factor analysis-dennoised images. *Nucl Med Biol* 2014; 41: 186–195.
39. Tsartsalis S, Tournier BB, Aoun K, et al. A single-scan protocol for absolute D2/3 receptor quantification with [123I]IBZM SPECT. *Neuroimage* 2017; 147: 461–472.
40. Schwarz JM. Using fluorescence activated cell sorting to examine cell-type-specific gene expression in rat brain tissue. *J Vis Exp* 2015; e52537.
41. Altman DG. *Practical statistics for medical research*. London, UK: Chapman & Hall 1991: 455–460.
42. Chaney A, Bauer M, Bochicchio D, et al. Longitudinal investigation of neuroinflammation and metabolite profiles in the APPswe xPS1Deltae9 transgenic mouse model of Alzheimer's disease. *J Neurochem* 2018; 144: 318–335.
43. Repalli J. Translocator protein (TSPO) role in aging and Alzheimer's disease. *Curr Aging Sci* 2014; 7: 168–175.
44. Serriere S, Tauber C, Vercouillie J, et al. Amyloid load and translocator protein 18 kDa in APPswePS1-dE9 mice: a longitudinal study. *Neurobiol Aging* 2015; 36: 1639–1652.
45. Betlazar C, Harrison-Brown M, Middleton RJ, et al. Cellular sources and regional variations in the expression of the neuroinflammatory marker translocator protein (TSPO) in the normal brain. *Int J Mol Sci* 2018; 19.
46. Albrecht DS, Granziera C, Hooker JM, et al. In vivo imaging of human neuroinflammation. *ACS Chem Neurosci* 2016; 7: 470–483.
47. Cosenza-Nashat M, Zhao ML, Suh HS, et al. Expression of the translocator protein of 18 kDa by microglia, macrophages and astrocytes based on immunohistochemical localization in abnormal human brain. *Neuropathol Appl Neurobiol* 2009; 35: 306–328.
48. Mirzaei N, Tang SP, Ashworth S, et al. In vivo imaging of microglial activation by positron emission tomography with [(11)C]PBR28 in the 5XFAD model of Alzheimer's disease. *Glia* 2016; 64: 993–1006.
49. Gonzalez-Reyes RE, Nava-Mesa MO, Vargas-Sanchez K, et al. Involvement of astrocytes in Alzheimer's disease from a neuroinflammatory and oxidative stress perspective. *Front Mol Neurosci* 2017; 10: 427.
50. Solito E and Sastre M. Microglia function in Alzheimer's disease. *Front Pharmacol* 2012; 3: 14.
51. Verkhratsky A, Olabarria M, Noristani HN, et al. Astrocytes in Alzheimer's disease. *Neurotherapeutics* 2010; 7: 399–412.
52. McGuinness B, Gibney SM, Beumer W, et al. Exaggerated increases in microglia proliferation, brain inflammatory response and sickness behaviour upon lipopolysaccharide stimulation in non-obese diabetic mice. *Neuroimmunomodulation* 2016; 23: 137–150.
53. Gomez-Nicola D and Perry VH. Analysis of microglial proliferation in Alzheimer's disease. *Methods Mol Biol* 2016; 1303: 185–193.
54. Gomez-Nicola D and Boche D. Post-mortem analysis of neuroinflammatory changes in human Alzheimer's disease. *Alzheimers Res Ther* 2015; 7: 42.
55. Serrano-Pozo A, Gomez-Isla T, Growdon JH, et al. A phenotypic change but not proliferation underlies glial responses in Alzheimer disease. *Am J Pathol* 2013; 182: 2332–2344.
56. Nirzhor SSR, Khan RI and Neelotpol S. The biology of glial cells and their complex roles in Alzheimer's disease: new opportunities in therapy. *Biomolecules* 2018; 8.
57. Marlatt MW, Bauer J, Aronica E, et al. Proliferation in the Alzheimer hippocampus is due to microglia, not astroglia, and occurs at sites of amyloid deposition. *Neural Plast* 2014; 2014: 693851.
58. Khan ZU, Koulou P, Rubinstein M, et al. An astroglia-linked dopamine D2-receptor action in prefrontal cortex. *Proc Natl Acad Sci U S A* 2001; 98: 1964–1969.
59. Huck JH, Freyer D, Bottcher C, et al. De novo expression of dopamine D2 receptors on microglia after stroke. *J Cereb Blood Flow Metab* 2015; 35: 1804–1811.
60. Sharma G and Vijayaraghavan S. Nicotinic cholinergic signaling in hippocampal astrocytes involves calcium-induced calcium release from intracellular stores. *Proc Natl Acad Sci U S A* 2001; 98: 4148–4153.
61. Shytle RD, Mori T, Townsend K, et al. Cholinergic modulation of microglial activation by alpha 7 nicotinic receptors. *J Neurochem* 2004; 89: 337–343.